Internal spin-wave confinement in magnetic nanowires due to zig-zag shaped magnetization

Jesco Topp, Jan Podbielski, and Detlef Heitmann
Institut für Angewandte Physik und Mikrostrukturforschungszentrum, Universität Hamburg, Jungiusstrasse 11, D-20355 Hamburg, Germany

Dirk Grundler*
Physik-Department E10, Fakultät für Physik, Technische Universität München, James-Franck-Strasse, D-84748 Garching, Germany
(Received 2 April 2008; published 23 July 2008)

We perform broadband spin-wave spectroscopy on thin submicrometer-wide $Ni_{80}Fe_{20}$ magnetic wires. Intentionally, we apply the in-plane magnetic field under an angle that is a few degrees off with respect to the in-plane hard-axis direction. In an intermediate field regime we find dipole-exchange modes that, as substantiated by micromagnetic simulations, reflect spin waves in intrinsically formed nanometer-wide channels along the wire. Interestingly, this phenomenon is not ruled by the outer boundary conditions at the geometrical edges but by a deterministic zig-zag shaped magnetization configuration that varies on the nanometer scale in the inner part of the wire. In our case the individual channel width is only 65 nm, about a factor of five smaller than the geometrical width of 300 nm. Internal spin-wave guiding becomes possible, resembling the graded-index approach for optical wave guiding in fibers. This opens new perspectives for spin-wave propagation in magnonic waveguides.

DOI: 10.1103/PhysRevB.78.024431 PACS number(s): 75.75.+a, 75.30.Ds, 75.50.Bb, 76.50.+g

I. INTRODUCTION

Micron- and submicron-wide magnetic wires have attracted considerable interest very recently due to both a data storage technology[1] and intriguing spin-wave physics such as quantization,[2] interference,[3,4] filtering,[5] and self-focusing of spin waves.[6] Studies were carried out on thin magnetic wires, which were magnetized either along the in-plane easy or hard axis, i.e., these were longitudinally and transversely magnetized wires, respectively.[2,5–11] Intermediate angles for the applied in-plane field $\vec{H}$ have been avoided since complex hysteresis loops and magnetic configurations $\vec{M}(x,y)$ follow. (x and y are orthogonal in-plane directions.) Unintentional edge roughness of a real wire might change the switching characteristics from device to device.[12] Involved and hysteretic spin-wave resonances are expected since they are known to reflect local variations of $\vec{M}(x,y)$ and the magnetic history in a sensitive manner.[13,14] A finite slope and surface anisotropy at edges have already been found to reduce significantly the saturation field. A reduction of a factor of two and more has been demonstrated for *nonideal* edges in Ref. 9 if compared to *ideal* edges. In this paper we report spin waves observed in Permalloy wires where $\vec{H}$ is applied a few degrees off with respect to the hard-axis direction. In a wide magnetic-field regime, we find that $\vec{M}(x,y)$, reflecting a buckling state, is inhomogeneous on the nanometer scale. Interestingly, a prominent spin-wave mode occurs. Micromagnetic simulations substantiate that this mode is confined to two nanometer-wide regions within the wire. It is different from previously reported center and edge modes.[7,8] In our case, due to the zig-zag shaped $\vec{M}(x,y)$, the intrinsic spin-wave channel forms where, in a propagation experiment,[6,10,11] the spin wave will be confined and, consequently, guided along the wire. In particular, the channel is *offset* from the geometrical edges. The discovered *internal* confinement in magnetic nanowires opens interesting perspectives for spin-dynamics research and magnonic applications.[3,5] It resembles the guiding of optical modes in graded-index fibers and might lead to a similar breakthrough in magnetic data transmission, as it has occurred for optical communication.

This paper is organized as follows: in Sec. II we describe the broadband spin-wave spectroscopy, measurement configuration, and original data. In Sec. III we present simulations on the quasistatic magnetization configuration $\vec{M}(x,y)$ and internal field $\vec{H}_{\mathrm{int}}(x,y)$. Calculated spectra and comparison with experiments are discussed in Sec. IV. In Sec. V we conclude.

II. SPIN-WAVE SPECTROSCOPY

We investigated arrays of different 20-nm-thick and 140-μm-long $Ni_{80}Fe_{20}$ (Permalloy) wires using broadband spin-wave spectroscopy (cf. Fig. 1). Each array contained 185 magnetic wires prepared by electron-beam lithography and lift-off processing on a GaAs substrate. Here we focus on wires with $w=300$ nm. The spacing between the wires was 700 nm to minimize dipolar interactions. By the number of 185 wires, we (i) increased the signal-to-noise ratio and (ii) investigated the averaged behavior of an ensemble of nominally identical wires, i.e., the data reflected the fundamental behavior of the individual magnetic wire. Spin-wave spectroscopy was carried out in the linear regime[15] by means of transmission measurements performed on a coplanar waveguide (CPW) integrated on top of the array [Figs. 1(a) and 1(b)]. The scattering parameters were measured by a vector-network analyzer (VNA) and exhibited absorption features when the excitation frequency f coincided with a spin-wave eigenfrequency. A detailed description of the VNA technique is found in Refs. 4 and 14. Between the

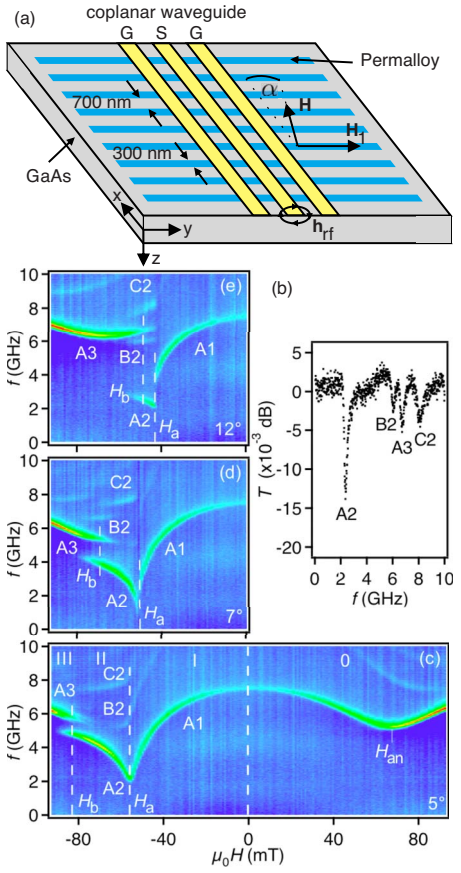

FIG. 1. (Color online) (a) Sketch of the experiment: Au leads form ground (g) and signal (s) lines on top of the Permalloy nanowires. Parameters are defined in the figure. (b) Transmission spectrum $T(f)$ obtained on an array with 185 Permalloy wires with $w=300$ nm at $\alpha=12°$ and $\mu_0 H=-46$ mT. This spectrum belongs to regime II in the experiment since $\mu_0 H_{b,\mathrm{exp}}=-44$ mT at $\alpha=12°$. Color-coded spectra for (c) $\alpha=5°$, (d) 7°, and (e) 12° (bright means strong absorption). Labels are discussed in the text.

Permalloy and the CPW a 50–nm-thick insulating layer of SiO_2 was deposited. The sample resided within a gigahertz probe station equipped with two pairs of coils. We applied the in-plane field $\vec{H}=(H_x,H_y)$ under a specific angle α with respect to the CPW's central conductor, which was perpendicular to the wires' long axis [Fig. 1(a)]. The microwave field $\vec{h}_{rf}$ excited spin-wave modes confined in x direction and propagating in $\pm y$ direction.[16] Spin-wave propagation under such experimental conditions was evidenced in Refs. 6, 10, and 11 using spatially resolved spectroscopy. In the following we discuss the field dependencies of modes, i.e., the so-called magnetic-field dispersions. Reference spectra have first been measured between +90 and −90 mT for $\alpha=0$ (not shown). For $\alpha=0$, $\vec{H}$ is along the x direction. We find the pronounced center mode reported previously.[8] It exists over the whole field range. The field dependent eigenfrequency reflects the well-known hard-axis behavior of an anisotropic micromagnet[9,17] with a frequency minimum when $|H|$ equals the anisotropy field H_{an} (here about 60 mT). The magnetic-field dispersion is, in particular, symmetric with respect to $H=0$. The center mode exhibits the largest spin-precession amplitude right in the center of the wire. Only at the edge, the amplitude is reduced due to dipolar pinning. Simulations, which we will discuss later, show a value of 17%–25% at the edge if compared to the central amplitude, depending on the magnetic field H.

We now turn to Fig. 1(c) where we find an asymmetric dispersion for $\alpha\neq 0$. Bright colors encode strong absorption at spin-wave eigenfrequencies. In a misaligned field $\vec{H}$, we distinguish four regimes 0–III. Tilting the field to $\alpha\neq 0$ introduces a component H_y that is collinear with the wire's easy axis. This component renders the hysteresis of an individual wire asymmetric with respect to $H=0$. The asymmetry becomes clearly visible for the array if the 185 wires experience a two-stepped magnetic history consisting of $\mu_0 H_1=+100$ mT at $\alpha=90°$ and $\mu_0 H_2=0$ prior to each measured spectrum. We use this history to align all wires along the easy axis in the same direction. Then we find the four different regimes 0–III in the field dispersions, and two clear switching (transition) fields H_a and H_b. At these fields, characteristic modes such as A1 to A3 change more or less abruptly.[13,14] Regime 0, i.e., $\mu_0 H>0$, is consistent with the hard-axis behavior discussed above for $\alpha=0$. In this regime (positive values of α and H), the component H_y has the same direction as H_1. The magnetization follows gradually the increasing field H. The frequency minimum at H_{an} is less pronounced since H and the hard axis are not exactly collinear.[17] This regime is well understood and not discussed here.[18]

We focus on regimes I–III, partitioned by H_a and H_b. The absolute values of both transition fields decrease with increasing angle α [Figs. 1(c)–1(e)]. At the same time the interval $[H_a;H_b]$ decreases, i.e., regime II becomes smaller. This regime II will turn out to be very interesting as it reflects the formation of a spin-wave mode confined on a deep-submicrometer length scale in x direction. The observation does not depend on the exact value of α as regime II is present in all three graphs of Figs. 1(c)–1(e). Interestingly the transition at H_a is sharp, whereas this is not the case for H_b. As we will show later, the transition at H_b is caused by the irreversible switching of $\vec{M}(x,y)$, very close to the geometrical edges. As this process depends on the edge roughness, each real wire has its own individual switching field H_b. The transition for the whole array thus needs several mT. Consistently, we observe a successive transfer of intensity from the low-frequency (A2) to the high-frequency (A3) mode as a function of H. In the following, we define H_b as the field where modes A2 and A3 have the same intensity. The absolute value of H_b decreases with increasing angle α due to a more negative H_y. The sharp transition at H_a indicates that the underlying switching event occurs for nearly all individual wires at the same applied field. This already suggests that not the edges but the central part is relevant. H_a also decreases with increasing angle α although more slowly than H_b.[19] We have found that in the intermediate field range $H_b<H<H_a$, spin-wave eigenmodes (A2–C2) exist with unique properties, which have not been explored so far. Before we discuss spin-precession profiles in regime II, it is instructive to review the switching processes by means of micromagnetic simulations.

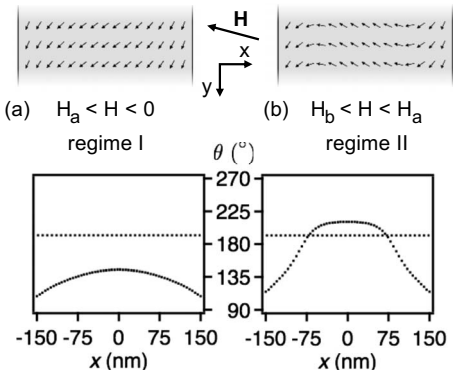

FIG. 2. (Top) Magnetization $\vec{M}(x,y)$ in two different fields H with $\alpha=12°$. The wire was initially saturated along the y direction: (a) $\mu_0 H=-44$ mT and (b) -48 mT. Small arrows indicate local magnetic moments. (Bottom) Angle $\theta(x)$, i.e., the orientation of spins relative to the x axis across the wire. The broken line is at $(180°+12°)$, i.e., the orientation of $\vec{H}$.

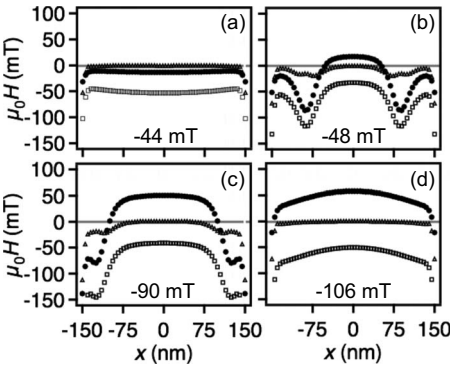

FIG. 3. [(a)–(d)] Spatially resolved internal (solid dots), demagnetization (open squares), and exchange fields (open triangles) at $\alpha=12°$ for H. In (b) $H_{\rm int}$ reenters large negative values in localized regions of the wire. They promote spin-wave confinement in x direction that is, in particular, *offset* from the edges. Propagation in y direction is possible.

III. MICROMAGNETIC SIMULATIONS

We use the OOMMF micromagnetic code[20] and apply the one-dimensional (1D) periodic-boundary-condition extension[21] to model an infinitely long magnetic wire. The simulated segment has $\Delta x\times\Delta y\times\Delta z$ equal to $300\times100\times19.5$ nm^3. The OOMMF discretization uses a cell of $5\times25\times6.5$ nm^3.[22] In the thin and narrow wire, the remanent magnetization aligns itself along the long axis, i.e., the easy axis. If we apply a field $\vec{H}$ with $\alpha\neq0$, two switching processes at fields H_a and H_b are found, which is consistent with the experiment. Decreasing H from $H=0$, the magnetization in the center follows the applied field more easily than at the edges. $\vec{M}$ is no longer uniform in y direction [Fig. 2(a)]. The component H_y is essential for the switching: for $H_a<H<0$ (regime I), the field component H_y and the global $\vec{M}$ point in different directions. At $H=H_a$ the component H_y induces a reversal in the wire's center [Fig. 2(b)]. For $H_b<H<H_a$ (regime II), spins in the central region of the wire tend to point in $\vec{H}$ direction, however, they are not strictly collinear with $\vec{H}$. The edge regions exhibit a nearly unaltered magnetic configuration [cf. angle θ in Fig. 2(b)]. The transition field H_a indicates the switching of the central $\vec{M}(x,y)$. As a consequence, a buckling magnetization state with a zig-zag shaped configuration $\vec{M}(x,y)$ is formed in regime II. The increase in exchange energy is compensated by a reduction in Zeeman energy as the microscopic magnetic moments around $x=0$ align with $\vec{H}$. Despite the inhomogeneous $\vec{M}(x,y)$, the resonance feature A2 in regime II is pronounced and sharp [cf. Fig. 1(b)]. At $H=H_b$ the component H_y is sufficient to induce also the edges' reversal. The wire enters regime III and, for $H<H_b$, acquires a similar configuration $\vec{M}(x,y)$ like in regime 0 for $H>H_{an}$ (not shown). For infinitely long 300-nm-wide wires with ideal edges, the two switching fields are numerically determined to be: $\mu_0 H_a=-47$ mT and $\mu_0 H_b=-105$ mT at $\alpha=12°$.

To understand the microscopic nature of modes A2–C2, it is helpful to analyze in detail the inhomogeneous internal field $\vec{H}_{\rm int}(x,y)$. This field is known to be relevant for spin waves in micromagnets.[7,13] In each discretization cell, the internal field $\vec{H}_{\rm int}(x,y)$ is collinear with the magnetization $\vec{M}(x,y)$. In particular $\vec{H}_{\rm int}(x',y')$ is antiparallel to $\vec{M}(x',y')$ as long as switching has not yet occurred at position (x',y'). It is parallel in the aligned and saturated cells. To describe the two different relative orientations, we use negative and positive values for $H_{\rm int}$ in Fig. 3. Demagnetization and exchange fields, which enter $\vec{H}_{\rm int}$, are not necessarily collinear to $\vec{M}$. The displayed curves thus reflect only the local strength. The negative sign is chosen for illustration purposes. For $H>H_a$ but close to H_a, the demagnetization field H_{dm} almost completely neutralizes the applied field. Apart from the edges, the internal field does not vary much with x and is -13 mT in Fig. 3(a). The exchange field H_{ex} is vanishingly small at -3 mT. For $H_b<H<H_a$, the internal field landscape has dramatically changed and has become inhomogeneous on the nanometer scale [Fig. 3(b)]. It features two distinct, sharp minima, separated by a central region of positive $H_{\rm int}$. The minima of -86 mT are at $x\approx\pm80$ nm. Locally, $H_{\rm int}$ is six times lower than in the prereversed state [Fig. 3(a)]. The spatial variation and amplitude of $H_{\rm int}$ reflect H_{dm} originating from the highly nonuniform magnetization distribution across the wire [Fig. 2(b)]. H_{dm} originates conceptually from pseudomagnetic charges, i.e., uncompensated spins. In regime I these lie at the edges of the structure. In regime II, however, the nonuniform $\vec{M}(x,y)$ produces uncompensated spins in the wire's interior, similar to a Néel-type domain wall. They enlarge the total magnetic charge and the magnitude of H_{dm}. We observe that two nanometer-wide dips of minimum $H_{\rm int}$ form in the already nanopatterned wire. Each dip extends in y direction and represents a channel for spin-wave confinement. Due to $\vec{H}_{ex}=(2A/\mu_0 M_s^2)\nabla^2\vec{M}$, the zig-zag shaped $\vec{M}(x,y)$ also enhances locally the exchange field up to $\mu_0|H_{ex}|=20$ mT. Approaching H_b enlarges the reversed region in the wire's center. The minima in $H_{\rm int}$ become deeper and move toward the geometrical edges [Fig. 3(c)]. For $H<H_b$, shown in Fig. 3(d),

the internal field revisits a nearly constant behavior. Apart from the edges, it exhibits a positive value and displays only a single shallow maximum in the center.

IV. CALCULATED SPIN-WAVE SPECTRA AND DISCUSSION

Starting from the quasistatic configurations we have performed dynamic simulations to numerically calculate the eigenmode spectrum. For this a field pulse $\vec{h}_{rf}$ of amplitude 1 mT and temporal full-width-half-maximum value 6 ps was applied. We tilted $\vec{h}_{rf}$ by 45° off from the in-plane direction. This means that we went beyond symmetry arguments discussed in the literature for CPWs,[23] which restricted the excitation of characteristic modes. As a reference, we have varied the orientation of $\vec{h}_{rf}$ in further simulations. We observed changes in the total oscillator strength of modes but not in the mode profiles that are discussed later. To remodel the long-wavelength limit in y direction, $\vec{h}_{rf}$ was homogeneous. The spatially resolved discrete Fourier transform of $M_z(x,y)$ was then analyzed. We averaged the data and thereby obtained resonance frequencies of eigenmodes with an even spatial symmetry. This rebuilt the CPW's detection mechanism.

We find that simulated and measured magnetic-field dispersions for the different angles α used in Figs. 1(c)–1(e) agree well with each other. The agreement is, in particular, true for the eigenfrequencies and absorption strengths. In our discussion, we will focus on $\alpha=12°$. Simulated data are depicted in Fig. 4. The switching field H_a of the center magnetization is modeled rather accurately. The difference is only 3 mT. Only the switching field H_b is predicted to be $\mu_0 H_b = -105$ mT. The experimentally observed value of −52 mT is a factor of two smaller. We attribute this remaining discrepancy to the edge reversal process in real wires exhibiting a finite edge slope, roughness, and inhomogeneities. Edge reversal has been found to depend critically on the exact geometry and properties of the edges.[9,12] Our simulations assume an ideal edge with no roughness, which certainly does not hold in the experiment. Simulations performed in Ref. 9, assuming nonideal edges reported a discrepancy of up to about a factor of two, similar to our finding. Importantly, H_b is still appreciably different from H_a such that we observe regime II clearly in our experiment on nanowires. In both experiment and simulation, we find three characteristic modes A2–C2. The interesting regime II covers a broader regime in H for small angles α [Figs. 1(c) and 1(d)]. In the following we will discuss the spin-wave confinement discovered in this work on the basis of Fig. 4 where regime II is shown for the wire with ideal edges.

Fourier-transform imaging is now used to analyze the spatial mode profile and phase of spin-precession amplitudes.[24] The mode profiles A1 and A3, shown for $\alpha=12°$ in Fig. 4, are valid in regimes I and III, respectively. They are consistent with the center modes, which have been discussed in earlier publications for $\alpha=0$. These modes reflect coherent precession of spins where dipolar pinning reduces the spin-wave amplitude partly at the geometrical edges.[25] This leads

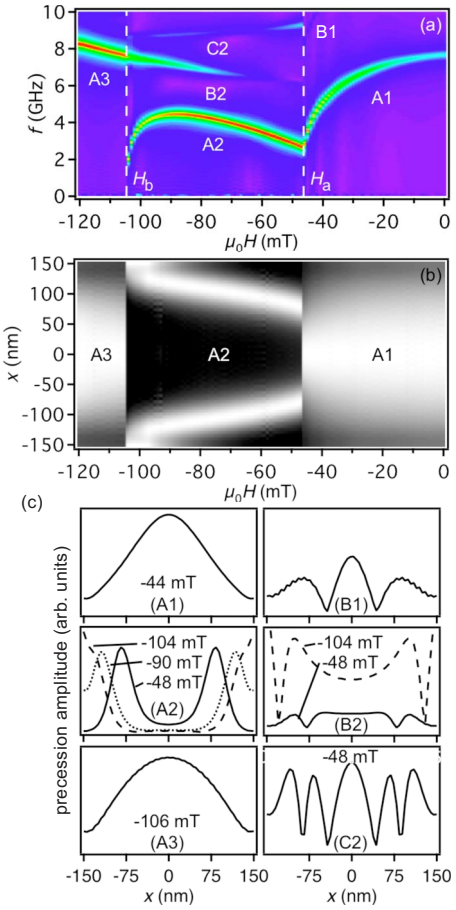

FIG. 4. (Color online) (a) Simulated magnetic-field dispersion for a single 300-nm-wide wire with H tilted by $\alpha=12°$ from the x direction. (b) Spin-precession intensity across the nanowire for modes A1–A3 as a function of x (vertical axis) at the same fields H shown in (a) (white represents a large value). The spin-wave confinement in regime II, originating from the zig-zag shaped $\vec{M}(x,y)$, is clearly seen. For each H, the maximum amplitude is normalized to one for illustration purposes. Bottom: Fourier-transform images (linescans) illustrating the spin-precession intensity along x direction (horizontal axis) at specific fields. Here, we also show higher order modes. The labels refer to the different modes discussed in the text.

to bell-shaped profiles as a function of x. The gray-scaled plot in Fig. 4(b) demonstrates that this profile exists for $H < H_b$ and $H > H_a$. For $H_b < H < H_a$ (regime II), the scenario is strikingly different. Here the profile A2 in Fig. 4(b) consists of two narrow spin-precession peaks. At −48 mT, e.g., the full-width-half-maximum value is 65 nm for each peak, far smaller than the geometry imposes. The corresponding wave vector $k_x \approx 5 \cdot 10^5$ cm^{-1} is large. The existence of such dipole-exchange spin waves is correlated with the zig-zag shaped $\vec{M}(x,y)$, producing narrow minima in H_{int}. They form a nanometer-wide twin-guide channel, which is offset from the edges and extends in y direction. The central spins of the wire are merely excited. The spin-precession amplitudes at both edges are, in particular, small and close to zero ($\leq 5\%$) at $\mu_0 H = -48$ mT. This feature is in contrast to modes A1 and A3, which exhibit a larger amplitude at the edges. It

substantiates that the confinement results from a different microscopic mechanism. The reduced amplitudes at the geometrical edges might suggest smaller magnon scattering due to edge roughness for A2 than for the center modes. This remains to be evidenced in a propagation experiment. The precession peaks in regime II move toward the edges with decreasing H. This is highlighted in the central part of Fig. 4(b).

A detailed analysis based on the simulation of the *minor-loop behavior*[14] provides that the eigenfrequencies of modes A1 and A2 can be *degenerate* at $\mu_0 H \cong -46$ mT despite the very different underlaying magnetization configurations $\vec{M}(x,y)$ and spin-precession amplitudes. In the simulation, a discontinuous *upward* frequency jump from A1 to A2 occurs at the transition field of −47 mT. At −46(46.7)mT the simulations gives 2.83(1.31) GHz for A1 in regime I, reflecting a soft-mode behavior. For A2 we find 2.59(2.63) GHz at the same fields. The eigenfrequencies of A1 and A2 thus cross. The clear *downward* jump seen in the experiment for $\alpha = 12°$ might therefore be due to the variation of $\mu_0 H$ in finite steps of 1 mT. The predicted degeneracy point remains to be evidenced experimentally.

Mode B1 of regime I is the first higher order mode of A1 with even spatial symmetry. It exhibits three regions of large amplitude: two at the sides of the wire and one in the center. Evaluation of the phase shows that the center and sides precess out of phase (not displayed). Due to this, the oscillator strength of B1 is small, causing a weak feature in Fig. 4(a). Mode B2 is a higher order mode of A2 in regime II. The number of precession peaks increases and the outer peaks shift more and more toward the edges for decreasing H. Mode C2 recovers a large amplitude at $x=0$. Interestingly, at $H=H_b$ the dispersion of mode B2 seems to transform into A3 of regime III continuously although there is a remarkable difference in profiles between B2 and A3. A soft behavior of mode B2 is not observed. The origin for the different degeneracies found in this work needs to be investigated further. Nanowires prepared with more ideal edges will certainly help through extending the experimental field range where regime II exists at $\alpha = 12°$.

V. CONCLUSIONS

We have shown that a zig-zag shaped magnetization configuration with tilted spins confines spin waves in nanometer-wide channels. Zig-zag shaped magnetic configurations might be realized inside a macroscopic ferromagnetic thin film through a prepatterned antiferromagnetic underlayer, which, via exchange biasing, orients spins in specific directions on the nm scale. Thus, in a propagation experiment, spin-wave guiding becomes possible without geometrical edges. Evanescent stray fields and magnon scattering due to rough edges are reduced. In this sense, our spin-wave guides resemble the graded-index optical fiber. Switching between a broad center mode and narrow spin-wave channels with a degenerate eigenfrequency might also be interesting for spin-wave manipulation, interference, and self-focusing effects in magnonic waveguides.

Note added. Recently Demidov *et al.*[26] reported on nano-optics with spin waves propagating in two beams along magnetic wires. The beams followed from modes reported in Ref. 8 and exhibited a width of 400–500 nm. We have shown that the mechanism outlined here allows us to form magnon waveguides, which exhibit a deep-submicrometer width (65 nm in our case). This provides a new nanoscale approach also for nano-optics with spin waves.

ACKNOWLEDGMENTS

This work was supported by the DFG through Sonderforschungsbereich 668. Financial support by the Excellence Cluster "Nanosystems Initiative Munich (NIM)" is gratefully acknowledged.

*grundler@ph.tum.de

[1] S. S. P. Parkin, US Patent No. 6,834,005 (2004).
[2] C. Mathieu *et al.*, Phys. Rev. Lett. **81**, 3968 (1998).
[3] R. Hertel, W. Wulfhekel, and J. Kirschner, Phys. Rev. Lett. **93**, 257202 (2004).
[4] J. Podbielski, F. Giesen, and D. Grundler, Phys. Rev. Lett. **96**, 167207 (2006).
[5] S. Choi, K.-S. Lee, K. Y. Guslienko, and S.-K. Kim, Phys. Rev. Lett. **98**, 087205 (2007).
[6] V. E. Demidov, S. O. Demokritov, K. Rott, P. Krzysteczko, and G. Reiss, Phys. Rev. B **77**, 064406 (2008).
[7] J. Jorzick, S. O. Demokritov, B. Hillebrands, M. Bailleul, C. Fermon, K. Y. Guslienko, A. N. Slavin, D. V. Berkov, and N. L. Gorn, Phys. Rev. Lett. **88**, 047204 (2002).
[8] J. P. Park, P. Eames, D. M. Engebretson, J. Berezovsky, and P. A. Crowell, Phys. Rev. Lett. **89**, 277201 (2002).
[9] R. D. McMichael and B. B. Maranville, Phys. Rev. B **74**, 024424 (2006).
[10] H. T. Nguyen, T. M. Nguyen, and M. G. Cottam, Phys. Rev. B **76**, 134413 (2007).
[11] M. P. Kostylev, G. Gubbiotti, J.-G. Hu, G. Carlotti, T. Ono, and R. L. Stamps, Phys. Rev. B **76**, 054422 (2007).
[12] R. Mattheis, K. Ramstöck, and J. McCord, IEEE Trans. Magn. **33**, 3993 (1997).
[13] F. Giesen, J. Podbielski, B. Botters, and D. Grundler, Phys. Rev. B **75**, 184428 (2007).
[14] F. Giesen, J. Podbielski, T. Korn, M. Steiner, A. van Staa, and D. Grundler, Appl. Phys. Lett. **86**, 112510 (2005).
[15] J. Podbielski, D. Heitmann, and D. Grundler, Phys. Rev. Lett. **99**, 207202 (2007).
[16] Both the CPW's width of 10 μm and assumed inhomogeneous microwave current distribution give rise to k_y of the order of 10^3 cm^{-1} (long-wavelength limit in y direction).
[17] J. Lindner and K. Baberschke, J. Phys.: Condens. Matter **15**, R193 (2003).
[18] Y. Roussigné, S. M. Chérif, and P. Moch, J. Magn. Magn. Mater.

268, 89 (2004).
[19] B. B. Maranville, R. D. McMichael, C. L. Dennis, C. A. Ross, and J. Y. Cheng, IEEE Trans. Magn. **42**, 2951 (2006).
[20] M. J. Donahue and D. G. Porter (http://math.nist.gov/oommf/).
[21] K. Lebecki (http://info.ifpan.edu.pl/~lebecki/pbc.htm).
[22] The material parameters are $\mu_0 M_s = 1.08$ T (saturation magnetization), $A = 13 \cdot 10^{-12}$ J/m (exchange constant), and $\gamma = 176$ GHz/T (gyromagnetic ratio).
[23] X. Zhu, Z. Liu, V. Metlushko, P. Grütter, and M. Freeman, Phys. Rev. B **71**, 180408(R) (2005).
[24] M. Buess, R. Höllinger, T. Haug, K. Perzlmaier, U. Krey, D. Pescia, M. R. Scheinfein, D. Weiss, and C. H. Back, Phys. Rev. Lett. **93**, 077207 (2004).
[25] K. Y. Guslienko, S. O. Demokritov, B. Hillebrands, and A. N. Slavin, Phys. Rev. B **66**, 132402 (2002).
[26] V. Demidov *et al.*, Appl. Phys. Lett. **92**, 232503 (2008).